J. Plasma Phys. (2024), *vol*. 90, 975900201
Published by Cambridge University Press
doi:10.1017/S0022377824000266

Modelling a thrust imparted by a highly ionized magnetic nozzle rf plasma thruster

Kazunori Takahashi [1,2,†]

[1]Department of Electrical Engineering, Tohoku University, Sendai 980-8579, Japan

[2]National Institute for Fusion Science, Toki 509-5292, Japan

(Received 3 September 2023; revised 14 February 2024; accepted 15 February 2024)

Influence of the local-ionization-induced neutral depletion on the thrust imparted by the magnetic nozzle plasma thruster is discussed by simply considering reduction of the neutral density due to the ionization in the thruster model combining the global source model and the one-dimensional magnetic nozzle model. When increasing the rf power, it is shown that the increase rate of the plasma density is reduced, while the electron temperature continues to increase due to a decrease in the neutral density. Since the major components of the thrust are originated from the electron pressures in the source and in the magnetic nozzle, the increase in the electron temperature contributes to the increase in the thrust in addition to the gradual density increase by the rf power. The model qualitatively predicts the reduction of the thruster efficiency by the neutral depletion for the high-power condition, compared with the constant neutral density model.

Key words: plasma devices

1. Introduction

A magnetic nozzle radiofrequency plasma thruster has attracted much attention as an alternative option for high-power and long-lifetime electric propulsion devices (Charles 2009; Mazouffre 2016; Takahashi 2019), where a high-density plasma produced by an inductively coupled or wave-coupled plasma is transported along the applied magnetic field lines and expands in the divergent magnetic field, being called a magnetic nozzle. Physical phenomena occurring in the magnetic nozzle depend on the source plasma parameters, such as a plasma density, an electron temperature, an ion temperature, a plasma velocity, a discharge power and a neutral pressure. In the variable specific impulse plasma rocket having an ion cyclotron resonance heating section, most of the rf power is coupled with the ions and the ion temperature perpendicular to the magnetic field is much higher than the electron temperature (Longmier *et al.* 2014). The ion perpendicular energy is converted into the directed axial flow energy along the magnetic nozzle. For the case of a helicon thruster, the rf energy is used to heat the electrons and the electron impact ionization processes provide a high plasma density in the source. The plasma is transported along the axial magnetic field toward the source exit and then expands along the magnetic nozzle, where various plasma acceleration and momentum conversion processes have been

† Email address for correspondence: kazunori.takahashi.e8@tohoku.ac.jp

investigated so far. When applying the expanding magnetic field to the rf plasma source, a number of experiments have shown the spontaneous formations of the current-free double layer and the ambipolar electric field, both of which generate collimated supersonic ion beams (Charles & Boswell 2003; Cohen *et al.* 2003; Plihon, Chabert & Corr 2007). High energy electrons upstream of the potential drop can overcome the electric fields and neutralize the ion beams, while they are decelerated by the electric fields (Takahashi *et al.* 2007, 2011*a*). Therefore, the energy of the electrons is the source of the electric fields, and it is finally converted into the ion energy. Analytical, numerical and experimental studies have shown that the electron pressure balanced with the magnetic pressure of the magnetic nozzle is further converted into the axial thrust, which is equivalent to the Lorentz force due to the azimuthal diamagnetic current and the radial magnetic field (Fruchtman 2006; Ahedo & Merino 2010; Takahashi *et al.* 2011*b*; Fruchtman *et al.* 2012; Ahedo & Navarro-Cavallé 2013; Takahashi, Charles & Boswell 2013; Lafleur 2014; Emoto, Takahashi & Takao 2021). Therefore, the plasma parameters at the nozzle entrance and in the nozzle are a key issue to improve the thruster performance.

In fundamental laboratory experiments on the helicon plasma source, the saturation of the plasma density, i.e. the density limit, has been observed due to neutral depletion (Boswell 1984; Gilland, Breun & Hershkowitz 1998; Magee *et al.* 2013; Zhang *et al.* 2021). A theoretical model on the effect of the neutral depletion has been established in a simple geometry with no magnetic nozzle, implying the modification of the plasma density profile (Fruchtman *et al.* 2005; Fruchtman 2008). Such a behaviour has been experimentally confirmed in a magnetic nozzle plasma thruster configuration where the plasma density and potential near the thruster exit are reduced by the neutral depletion (Takahashi *et al.* 2015; Takahashi, Takao & Ando 2016*b*). Under this situation, a part of the axial ion momentum gained by the potential drop inside the source is often lost to the radial source wall, resulting in the performance degradation of the thruster. A simple thruster model using a particle balance, a power balance and a one-dimensional magnetic nozzle model has been used to qualitatively understand the thruster performance, assuming a weakly ionized condition (Takahashi 2022). In such a model the electron temperature is independent of the rf power, while the source plasma density is proportional to the rf power, giving a linear increase in the thrust by the rf power. However, the thrusts measured in experiments have shown a decrease in the slope of the thrust versus rf power characteristics for high-power conditions. This discrepancy is considered to be originated from the change in the neutral density in the source tube.

In the present paper the change in the neutral density due to the ionization is incorporated into the global source model, which are further coupled with the one-dimensional magnetic nozzle model assuming isothermal electrons. In order to qualitatively discuss the thrust versus rf power characteristic, the total thrust consisting of the pressure forces exerted to the source and the magnetic nozzle is calculated. The results are compared with those not taking the neutral depletion into account. These results show the decrease in the density and the increase in the electron temperature in the source; it is suggested that the total thrust and the thruster efficiency are resultantly reduced by the neutral depletion.

2. Theoretical model

Figure 1(*a*) shows the schematic diagram of the magnetic nozzle rf plasma thruster considered here. The source consists of an insulator glass source tube wound by an rf antenna and a solenoid placed near the thruster exit. The radius and length of the glass source tube are labelled as R_s and L_s, respectively. A magnetic field is applied to the source by supplying a dc current to the solenoid, where an axial profile of a

https://doi.org/10.1017/S0022377824000266 Published online by Cambridge University Press

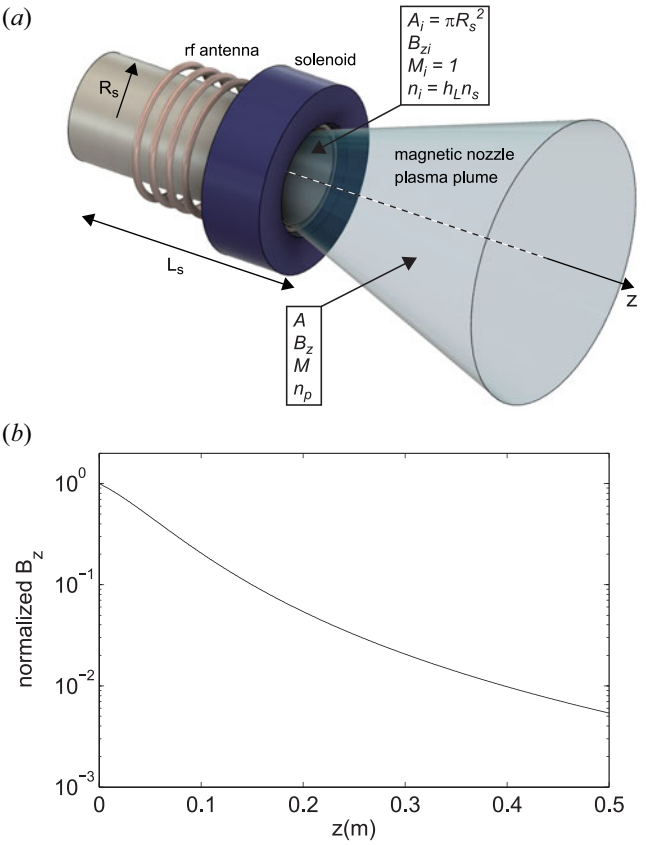

FIGURE 1. (*a*) Schematic diagram of the magnetic nozzle rf plasma thruster. (*b*) Typical axial profile of the normalized magnetic field on the z axis.

normalized magnetic field at the radial centre is plotted in figure 1(*b*). The field strength gradually decreases along the z axis ($z = 0$ is defined as the source exit and the magnetic nozzle entrance), i.e. the field lines geometrically expand, and the magnetic nozzle is formed downstream of the source. The cross-section of the plasma then expands along the magnetic nozzle as sketched in figure 1(*a*). In this section the global source model considering the ionization-induced decrease of the neutral density in argon plasma is coupled with the collisionless and isothermal one-dimensional magnetic nozzle model, where the Maxwellian electron energy distribution is considered.

The source model in argon is based on the well-known particle and power balance equations (Lieberman & Lichtenberg 2005) for spatially uniform profiles in the source. Assuming the Bohm velocity $u_B = (k_B T_e/m_{\mathrm{Ar}})^{1/2}$ of the ions at the wall sheath edge and at the open-source exit, the particle balance equation between the ionization in volume and the loss to the wall is given by

$$K_{\mathrm{iz}} n_g n_s V - n_s u_B A_{\mathrm{eff}} = 0, \tag{2.1}$$

where k_B, T_e, m_{Ar}, K_{iz}, n_g, n_s, $V = \pi R_s^2 L_s$ and A_{eff} are the Boltzmann constant, the electron temperature, the argon mass, the ionization rate constant, the neutral gas density, the plasma density in the source, the discharge volume and the effective loss area, respectively. The effective loss area A_{eff} is described by considering axial (h_L) and

https://doi.org/10.1017/S0022377824000266 Published online by Cambridge University Press

radial (h_R) centre-to-edge density ratios as

$$A_{\text{eff}} = 2\pi R_s^2 h_L + 2\pi R_s L_s h_R, \tag{2.2}$$

$$h_L = 0.86\left(3 + \frac{L_s}{2\lambda_i}\right)^{-1/2}, \tag{2.3}$$

$$h_R = 0.8\left(4 + \frac{R_s}{\lambda_i}\right)^{-1/2}, \tag{2.4}$$

where $\lambda_i = (n_g\sigma_i)^{-1}$ is the ion-neutral collisional mean-free path and the collisional cross-section of $\sigma_i = 1 \times 10^{-18}\,\text{m}^{-2}$ is used for the calculation. A typical mean-free path λ_i is about 10–25 cm for parameters used in § 3, being close to the source scale considered here. The centre-to-edge density ratios in (2.3) and (2.4) have been validated for such a condition as described in Lieberman & Lichtenberg (2005). The power lost from the system should be balanced with the input power P, i.e.

$$P = en_s u_B A_{\text{eff}} \varepsilon_T, \tag{2.5}$$

where $\varepsilon_T = \varepsilon_c + \varepsilon_e + \varepsilon_i$ is the total energy lost by the single electron-ion pair. Here ε_c, ε_e and ε_i are collisional (including ionization, excitation and elastic collisions), electron kinetic and ion kinetic energy losses, respectively, given by

$$\varepsilon_c = \varepsilon_{\text{iz}} + \frac{K_{\text{exc}}}{K_{\text{iz}}}\varepsilon_{\text{exc}} + 3\left(\frac{m_e}{m_{\text{Ar}}}\right)\left(\frac{K_{\text{el}}}{K_{\text{iz}}}\right)T_e, \tag{2.6}$$

$$\varepsilon_e = 2T_e \tag{2.7}$$

$$\varepsilon_i = 5.2T_e, \tag{2.8}$$

where approximated forms for the rate constants of K_{exc} (the excitation), K_{iz} (the ionization) and K_{el} (the elastic collision), which can be found in Lieberman & Lichtenberg (2005) and functions of T_e, are used for the calculation.

The initial neutral density n_{g0} in the source for the given mass flow rate m_{dot} of the argon gas is simply calculated from $m_{\text{dot}} = m_{\text{Ar}} n_{g0} v_n(\pi R_s^2)$, assuming the gas velocity of $v_n = 400\,\text{m}\,\text{s}^{-1}$. When considering the reduction of the neutral density by the ionization, the neutral density n_g during the discharge is described as $n_g = n_{g0} - n_s$. By combining with (2.5), the neutral density n_g and the mean-free path λ_i are given by

$$n_g = n_{g0} - \frac{P}{eu_B A_{\text{eff}} \varepsilon_T}, \tag{2.9}$$

$$\lambda_i^{-1} = \sigma_i\left(n_{g0} - \frac{P}{eu_B A_{\text{eff}} \varepsilon_T}\right). \tag{2.10}$$

Substituting (2.10) into (2.2), the effective loss area A_{eff} can be numerically calculated as a function of T_e; the left-hand side term of (2.1) is also calculated as a function of T_e by using A_{eff}. The electron temperature giving zero for the left-hand side term of (2.1) can be numerically obtained, which further gives the source plasma density n_s from (2.5).

The ion velocity u_{zi} and the plasma density n_i at the open-source exit corresponding to the nozzle entrance are assumed to be $u_{zi} = u_B$ and $n_i = h_L n_s$, respectively. Considering the isothermally expanding electrons ($T_e = const.$), the paraxial approximation of $B_z(r, z) \sim B_z(0, z)$ and the area expansion given by $B_z A = const.$, the previous analytical model has

https://doi.org/10.1017/S0022377824000266 Published online by Cambridge University Press

derived the axial profile of the ion velocity in the magnetic nozzle as (Fruchtman *et al.* 2012)

$$\frac{M^2 - M_i^2}{2} - \ln\left(\frac{M}{M_i}\right) = \ln\left(\frac{B_{zi}}{B_z}\right), \tag{2.11}$$

where M is the ion Mach number and the subscript i denotes the value at the nozzle entrance ($z = 0$). Since assuming the Bohm velocity at the nozzle entrance, $M_i = 1$ is used for the calculation. In a collisionless plasma in the magnetic nozzle, the ion flux integrated over the cross-section of the plume is conserved. The flux conservation gives the equation of

$$h_L n_s M_i u_B A_i = n_p M u_B A, \tag{2.12}$$

where n_p and A are the plasma density and the cross-section of the plasma plume.

By numerically solving (2.1)–(2.12), the source plasma density n_s, the electron temperature T_e and the plasma density in the magnetic nozzle can be obtained. According to the thrust model, the major components of the thrust exerted to the magnetic nozzle rf plasma thruster are the static pressure force T_s inside the source and the Lorentz force T_B due to the azimuthal electron diamagnetic current and the radial magnetic field. After rewriting these forces into the one-dimensional model, the thrust is given by

$$T_{\text{total}} = T_s + T_B, \tag{2.13}$$

$$T_s = n_s k_B T_e A_i, \tag{2.14}$$

$$T_B = -\int_0^z \frac{n_p(z) k_B T_e A(z)}{B_z(z)} \frac{\partial B_z(z)}{\partial z'} \mathrm{d}z'. \tag{2.15}$$

The second term T_B is the axial component of the electron pressure force exerted to the expanding nozzle, being equivalent to the volume integration of the Lorentz force as analytically demonstrated in the previous study (Fruchtman *et al.* 2012).

3. Results

Figure 2 shows typical axial profiles of (*a*) the plasma velocity u_z and (*b*) the plasma density n_p calculated for $P = 10\,\text{kW}$, $m_{\text{dot}} = 2\,\text{mg s}^{-1}$, $R_s = 5\,\text{cm}$, $L_s = 15\,\text{cm}$, where the blue dotted and red solid lines are the results for the constant neutral density (i.e. non-depletion) model ($n_g = n_{g0}$) and the neutral depletion model ($n_g = n_{g0} - n_s$), respectively. The particle and power balance equations in § 2 give the source plasma density n_s, the electron temperature T_e and the axial centre-to-edge density ratio h_L of $(n_s, T_e, h_L) \sim (7.1 \times 10^{18}\,\text{m}^{-3}, 8.3\,\text{eV}, 0.446)$ and $(4.4 \times 10^{18}\,\text{m}^{-3}, 11.8\,\text{eV}, 0.468)$ for the constant neutral density and neutral depletion models, respectively. Figure 2 clearly shows the continuous increase in the axial velocity and the decrease in the plasma density in the magnetic nozzle; the higher axial velocity u_z and the lower plasma density n_p can be obtained for the neutral depletion model (the solid lines). Since the ion Mach number M depends on only the magnetic field profile as can be seen in (2.11), the profile of M should be the same for the two cases. The change in the axial velocity in figure 2(*a*) is due to the change in the electron temperature T_e and the resultant change in the Bohm velocity. The value of the axial centre-to-edge density ratio h_L is very similar between the two models; the change in the density n_p in figure 2(*b*) is originated from the source plasma density n_s.

To qualitatively understand the influence of the neutral depletion induced by the local ionization, the source plasma density and the electron temperature are calculated as functions of the rf power as plotted in figures 3(*a*) and 3(*b*), respectively, for the non-depletion model (crosses) and the neutral depletion model (open squares). Dotted and

https://doi.org/10.1017/S0022377824000266 Published online by Cambridge University Press

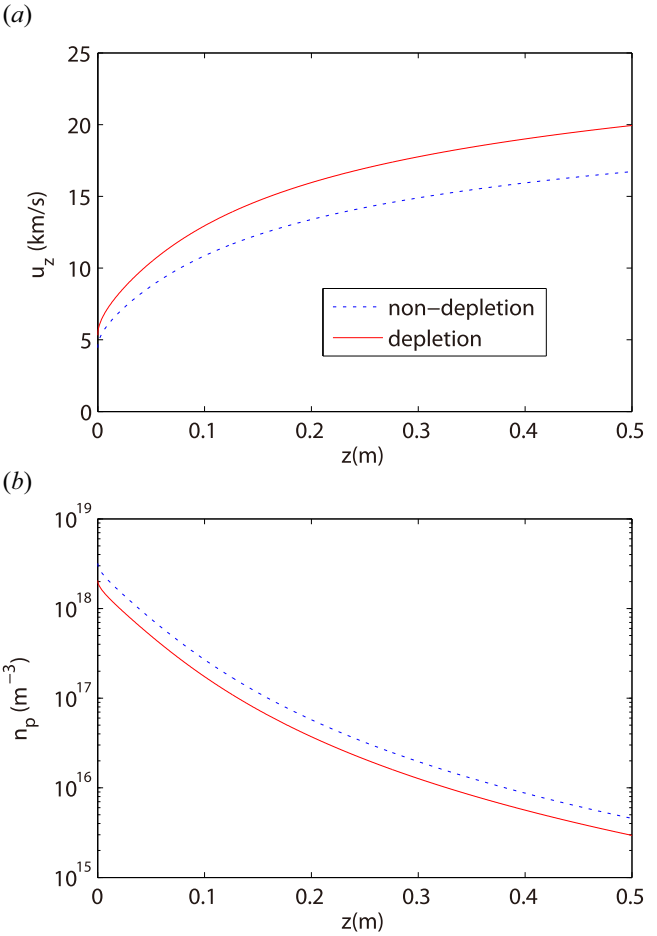

FIGURE 2. Axial profiles of (*a*) the plasma velocity u_z and (*b*) the plasma density n_p in the magnetic nozzle region for the non-depletion model (blue dotted lines) and for the neutral depletion model (red solid lines), where the rf power and the mass flow rate of the argon gas are chosen as $P_{\rm rf} = 10\,{\rm kW}$ and $m_{\rm dot} = 2\,{\rm mg\,s^{-1}}$, respectively.

solid lines in figure 3(*a*) denote the initial gas density n_{g0} for the given mass flow rate $m_{\rm dot}$ and the gas density n_g given by (2.9) in the neutral depletion model. In the non-depletion model the particle balance given by (2.1) is decoupled from the source plasma density n_s. Therefore, (2.1) solely gives the electron temperature, being constant for the given source geometry and the neutral density n_{g0} as seen in figure 3(*b*). Then the plasma density is found to be proportional to the discharge power as derived from (2.5) and as plotted by the crosses in figure 3(*a*). It is found that the plasma density exceeds the neutral gas density n_{g0} (the dotted line), which is out of touch with reality due to the lack of the discharge fuel in the low temperature and open system plasma. On the other hand, the plasma density in the neutral depletion model (the open squares) is significantly smaller than that for the non-depletion model; the electron temperature is contrarily increased for the high rf power conditions. It is found that the neutral density n_g decreases with an increase in the rf power due to the local ionization. In general, lowering the neutral gas density provides the high electron temperature due to the less collision between the electrons and neutrals. Reduction

https://doi.org/10.1017/S0022377824000266 Published online by Cambridge University Press

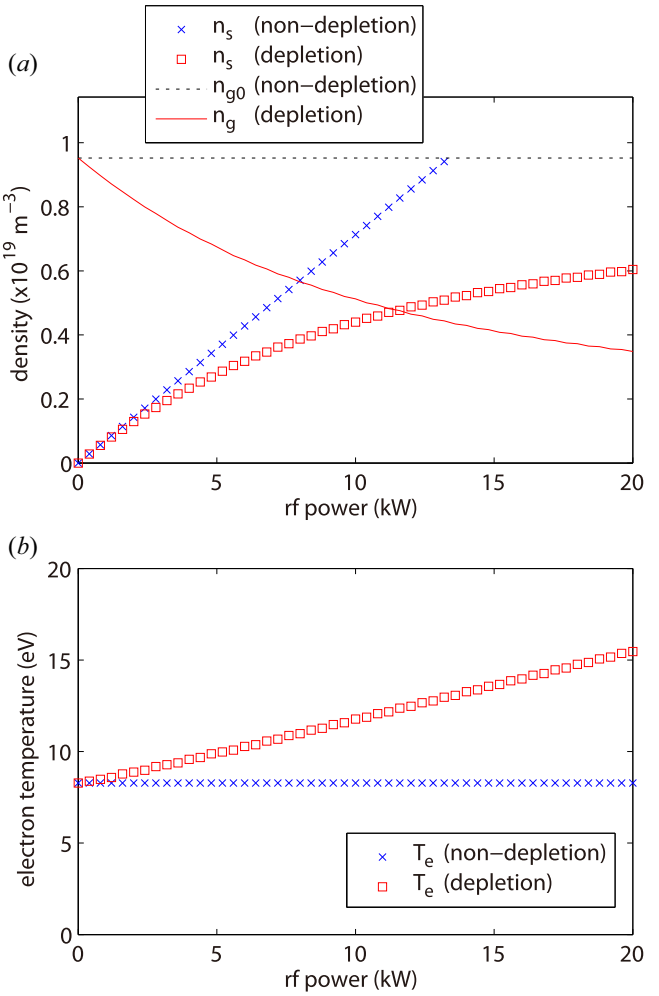

FIGURE 3. Plasma densities calculated from the non-depletion model (crosses) and from the neutral depletion model (open squares) as functions of the rf power, together with the initial neutral density n_{g0} (a black dotted line) and the neutral density n_g in the neutral depletion model (a red solid line). (*b*) Electron temperatures calculated from the non-depletion model (crosses) and from the neutral depletion model (open squares) as functions of the rf power. In these calculations, the mass flow rate is set at $m_{\rm dot} = 2\,{\rm mg\,s^{-1}}$.

of the background neutral density for the high plasma density condition provides the high electron temperature. Therefore, the rf power is used to heat the electrons rather than the ionization in the high discharge power conditions.

For the calculated source plasma density n_s and the electron temperature T_e, the thrust components given by (2.13)–(2.15) are calculated. Figure 4(*a*) shows the calculated T_s and T_B for the non-depletion model (T_s: open squares, T_B: crosses) and the neutral depletion model (T_s: open circles, T_B: stars). The total thrust $T_{\rm total}$ given by the sum of T_s and T_B are plotted in figure 4(*b*). It is noted that T_B is the function of z and continuously increases for the isothermal model. On the other hand, the electron temperature is typically cooled down along the z axis during the expansion since the electron energy is converted into the mechanical energy of the magnetic nozzle as discussed in terms of the thermodynamics

https://doi.org/10.1017/S0022377824000266 Published online by Cambridge University Press

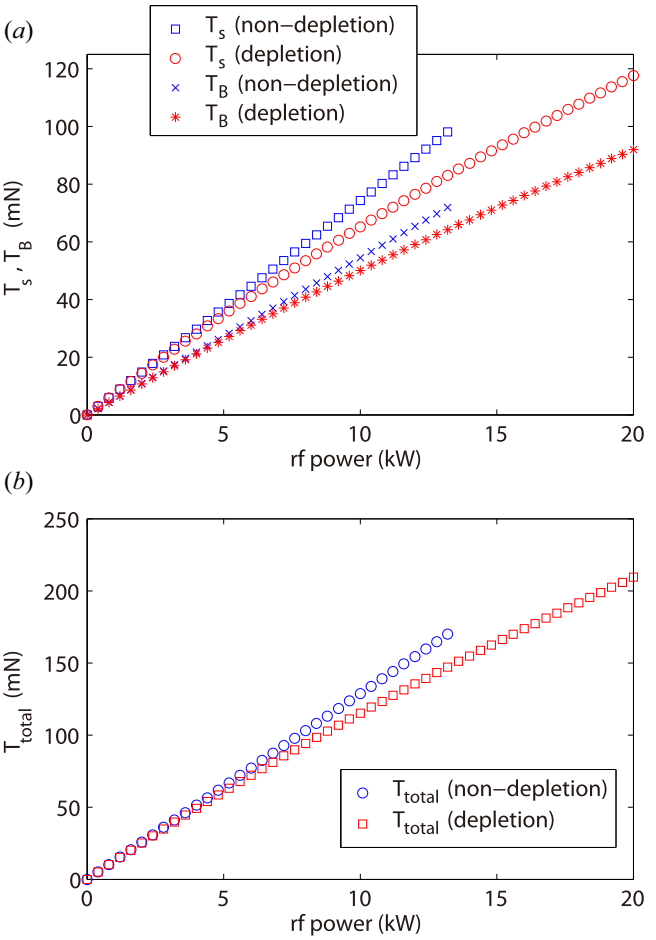

FIGURE 4. (*a*) Calculated T_s (open squares) and T_B (crosses) for the non-depletion model, and T_s (open circles) and T_B (stars) for the neutral depletion model for the same conditions as figure 3. (*b*) Total thrusts given by $T_{total} = T_s + T_B$ for the non-depletion model (open circles) and for the neutral depletion model (open squares) as functions of the rf power.

(Little & Choueiri 2016; Zhang, Charles & Boswell 2016; Kim *et al.* 2018; Takahashi *et al.* 2018, 2020*a*; Kim *et al.* 2023). Furthermore, the finally obtained thrust would depend on where the plasma is detached from the magnetic nozzle (Hooper 1993; Arefiev & Breizman 2005; Merino & Ahedo 2014; Takahashi & Ando 2017; Little & Choueiri 2019; Takahashi, Charles & Boswell 2022). Previous experiments have shown that both the T_B force and the momentum flux increase along the z axis over about 20–30 cm downstream of the thruster exit (Takahashi *et al.* 2016*a*; Takahashi, Sugawara & Ando 2020*b*). Therefore, the T_B force at $z = 30$ cm is taken here. The T_B force is found to be a major component of the thrust and is comparable to the T_s force, being consistent with the experiments (Takahashi *et al.* 2013). The T_s and T_B forces for the neutral depletion model (the open circles and the stars in figure 4*a*) are smaller than those for the non-depletion model (the open squares and the crosses in figure 4*a*), respectively. As a result, the total thrust, which is simply the sum of the two forces, is found to be reduced by considering the neutral depletion. It should be mentioned that the discrepancy between the two models is

https://doi.org/10.1017/S0022377824000266 Published online by Cambridge University Press

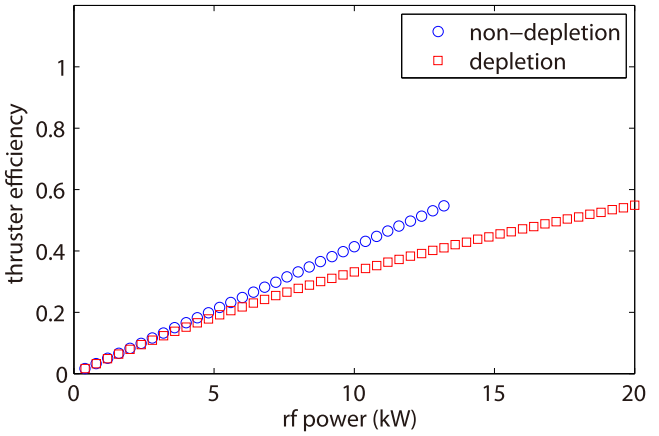

FIGURE 5. Thrust efficiencies for the non-depletion model (open circles) and for the neutral depletion model (open squares) as functions of the rf power for the same conditions as figure 3.

enhanced for the high-power condition as it is a result of the neutral depletion effect. As Fruchtman predicted and Takahashi *et al.* observed previously, the neutral depletion leads the asymmetric plasma density profile when introducing the gas from the upstream side of the source (Fruchtman 2008; Takahashi *et al.* 2016*b*), which provokes the loss of the axial ion momentum to the radial source wall and the thrust loss (Takahashi *et al.* 2015). However, the two-dimensional effect is not taken into account in the one-dimensional thruster model.

Thruster efficiency η_T is one of the important parameters to assess the thruster, which is generally given by

$$\eta_T = \frac{T_{\text{total}}^2}{2m_{\text{dot}}P}, \tag{3.1}$$

implying the ratio of the thrust energy to the input power. Figure 5 shows the calculated thruster efficiency η_T as a function of the power for the non-depletion model (open circles) and the neutral depletion model (open squares), showing the thruster efficiency lowered by the neutral depletion effect. It is seen that the slope of η_T versus P characteristic gets smaller for the high-power condition in the neutral depletion model. This trend seems to be consistent with the experiments, as the experimental assessment has shown the saturation of the thruster efficiency when increasing the rf power (Takahashi 2022).

It is noted once again that the Maxwellian electron energy distribution is considered here. However, the observed electron energy probability function is often non-Maxwellian and close to Druyvesteyn due to the non-local effect for low pressure and collisional effect for high pressure (Takahashi *et al.* 2007, 2011*a*; Boswell *et al.* 2015). On the other hand, the beam electrons having an energy close to a phase velocity of the helicon wave have been detected in a helicon discharge experiment before (Chen & Hershkowitz 1998). The shape of the electron energy distribution would impact on the energy loss in the source as investigated previously (Kim *et al.* 2014, 2015). Therefore, incorporation of the effect of the distribution function into the thruster model will provide further precise estimation of the thruster performance, which remains a further analytical issue.

https://doi.org/10.1017/S0022377824000266 Published online by Cambridge University Press

4. Conclusion

The change in the neutral density due to the ionization is considered in the magnetic nozzle rf plasma thruster model combining the global source model and the one-dimensional magnetic nozzle model. When considering the neutral depletion effect, the source plasma density significantly decreases for the high-power condition, being originated from the reduction of the fuel gas in the source. It is considered that the energy is alternatively used to heat the electrons in the source, providing the high electron temperature in the source, by which the imparted thrust can be increased by the rf power. The analyses predicted that the neutral depletion effect reduces the thrust and the thruster efficiency, compared with the non-depletion model, i.e. the constant neutral density model. These numerical investigations contribute to the qualitative understanding and prediction of the high-power plasma thruster performance.

Acknowledgements

Editor Cary Forest thanks the referees for their advice in evaluating this paper.

Funding

This work is partially supported by Grant-in-Aid for Scientific Research from the Japan Society for the Promotion of Science (grant number 23H05442); and Fusion Oriented Research for disruptive Science and Technology (FOREST) from Japan Science and Technology Agency (grant number JPMJFR212A).

Declaration of interests

The author report no conflict of interest.

Data availability statement

The data that support the findings of this study are available from the corresponding author upon reasonable request.

Author contributions

K.T. performed all of the work presented here, i.e. established the model and numerical code, interpreted the results and wrote the paper.

REFERENCES

AHEDO, E. & MERINO, M. 2010 Two-dimensional supersonic plasma acceleration in a magnetic nozzle. *Phys. Plasmas* **17** (7), 073501.

AHEDO, E. & NAVARRO-CAVALLÉ, J. 2013 Helicon thruster plasma modeling: two-dimensional fluid-dynamics and propulsive performances. *Phys. Plasmas* **20** (4), 043512.

AREFIEV, A.V. & BREIZMAN, B.N. 2005 Magnetohydrodynamic scenario of plasma detachment in a magnetic nozzle. *Phys. Plasmas* **12** (4), 043504.

BOSWELL, R.W. 1984 Very efficient plasma generation by whistler waves near the lower hybrid frequency. *Plasma Phys. Control. Fusion* **26** (10), 1147.

BOSWELL, R.W., TAKAHASHI, K., CHARLES, C. & KAGANOVICH, I.D. 2015 Non-local electron energy probability function in a plasma expanding along a magnetic nozzle. *Front. Phys*. **3**, 14.

CHARLES, C. 2009 Plasmas for spacecraft propulsion. *J. Phys.* D*: Appl. Phys*. **42** (16), 163001.

CHARLES, C. & BOSWELL, R. 2003 Current-free double-layer formation in a high-density helicon discharge. *Appl. Phys. Lett*. **82** (9), 1356–1358.

CHEN, R.T.S. & HERSHKOWITZ, N. 1998 Multiple electron beams generated by a helicon plasma discharge. *Phys. Rev. Lett*. **80**, 4677–4680.

COHEN, S.A., SIEFERT, N.S., STANGE, S., BOIVIN, R.F., SCIME, E.E. & LEVINTON, F.M. 2003 Ion acceleration in plasmas emerging from a helicon-heated magnetic-mirror device. *Phys. Plasmas* **10** (6), 2593–2598.

EMOTO, K., TAKAHASHI, K. & TAKAO, Y. 2021 Axial momentum gains of ions and electrons in magnetic nozzle acceleration. *Plasma Sources Sci. Technol*. **30** (11), 115016.

FRUCHTMAN, A. 2006 Electric field in a double layer and the imparted momentum. *Phys. Rev. Lett*. **96**, 065002.

FRUCHTMAN, A. 2008 Neutral depletion in a collisionless plasma. *IEEE Trans. Plasma Sci*. **36** (2), 403–413.

FRUCHTMAN, A., MAKRINICH, G., CHABERT, P. & RAX, J.M. 2005 Enhanced plasma transport due to neutral depletion. *Phys. Rev. Lett*. **95**, 115002.

FRUCHTMAN, A., TAKAHASHI, K., CHARLES, C. & BOSWELL, R.W. 2012 A magnetic nozzle calculation of the force on a plasma. *Phys. Plasmas* **19** (3), 033507.

GILLAND, J., BREUN, R. & HERSHKOWITZ, N. 1998 Neutral pumping in a helicon discharge. *Plasma Sources Sci. Technol*. **7** (3), 416.

HOOPER, E.B. 1993 Plasma detachment from a magnetic nozzle. *J. Propul. Power* **9** (5), 757–763.

KIM, J.Y., CHUNG, K.-J., TAKAHASHI, K., MERINO, M. & AHEDO, E. 2023 Kinetic electron cooling in magnetic nozzles: experiments and modeling. *Plasma Sources Sci. Technol*. **32** (7), 073001.

KIM, J.Y., CHUNG, K.S., KIM, S., RYU, J.H., CHUNG, K.-J. & HWANG, Y.S. 2018 Thermodynamics of a magnetically expanding plasma with isothermally behaving confined electrons. *New J. Phys*. **20** (6), 063033.

KIM, J.Y., KIM, D.-H., KIM, J.H., JEON, S.-B., CHO, S.-W. & CHUNG, C.-W. 2014 Power dependence of electron density at various pressures in inductively coupled plasmas. *Phys. Plasmas* **21** (11), 113505.

KIM, J.Y., KIM, Y.-C., KIM, Y.-S. & CHUNG, C.-W. 2015 Effect of the electron energy distribution on total energy loss with argon in inductively coupled plasmas. *Phys. Plasmas* **22** (1), 013501.

LAFLEUR, T. 2014 Helicon plasma thruster discharge model. *Phys. Plasmas* **21** (4), 043507.

LIEBERMAN, M.A. & LICHTENBERG, A.J. 2005 *Principles of Plasma Discharges and Materials Processing*, 2nd edn, chap. 10. John Wiley & Sons.

LITTLE, J.M. & CHOUEIRI, E.Y. 2016 Electron cooling in a magnetically expanding plasma. *Phys. Rev. Lett*. **117**, 225003.

LITTLE, J.M. & CHOUEIRI, E.Y. 2019 Electron demagnetization in a magnetically expanding plasma. *Phys. Rev. Lett*. **123**, 145001.

LONGMIER, B.W., SQUIRE, J.P., OLSEN, C.S., CASSADY, L.D., BALLENGER, M.G., CARTER, M.D., ILIN, A.V., GLOVER, T.W., MCCASKILL, G.E., CHANG DÍAZ, F.R., *et al.* 2014 Improved efficiency and throttling range of the vx-200 magnetoplasma thruster. *J. Propul. Power* **30** (1), 123–132.

MAGEE, R.M., GALANTE, M.E., CARR, J., LUSK, G., MCCARREN, D.W. & SCIME, E.E. 2013 Neutral depletion and the helicon density limit. *Phys. Plasmas* **20** (12), 123511.

MAZOUFFRE, S. 2016 Electric propulsion for satellites and spacecraft: established technologies and novel approaches. *Plasma Sources Sci. Technol*. **25** (3), 033002.

MERINO, M. & AHEDO, E. 2014 Plasma detachment in a propulsive magnetic nozzle via ion demagnetization. *Plasma Sources Sci. Technol*. **23** (3), 032001.

PLIHON, N., CHABERT, P. & CORR, C.S. 2007 Experimental investigation of double layers in expanding plasmas. *Phys. Plasmas* **14** (1), 013506.

TAKAHASHI, K. 2019 Helicon-type radiofrequency plasma thrusters and magnetic plasma nozzles. *Rev. Mod. Plasma Phys*. **3**, 3.

TAKAHASHI, K. 2022 Thirty percent conversion efficiency from radiofrequency power to thrust energy in a magnetic nozzle plasma thruster. *Sci. Rep*. **12**, 18618.

TAKAHASHI, K. & ANDO, A. 2017 Laboratory observation of a plasma-flow-state transition from diverging to stretching a magnetic nozzle. *Phys. Rev. Lett*. **118**, 225002.

TAKAHASHI, K., CHARLES, C., BOSWELL, R. & ANDO, A. 2018 Adiabatic expansion of electron gas in a magnetic nozzle. *Phys. Rev. Lett*. **120**, 045001.

TAKAHASHI, K., CHARLES, C. & BOSWELL, R.W. 2013 Approaching the theoretical limit of diamagnetic-induced momentum in a rapidly diverging magnetic nozzle. *Phys. Rev. Lett*. **110**, 195003.

TAKAHASHI, K., CHARLES, C. & BOSWELL, R.W. 2022 Wave-driven electron inward transport in a magnetic nozzle. *Sci. Rep*. **12**, 20137.

TAKAHASHI, K., CHARLES, C., BOSWELL, R.W. & ANDO, A. 2020*a* Thermodynamic analogy for electrons interacting with a magnetic nozzle. *Phys. Rev. Lett*. **125**, 165001.

TAKAHASHI, K., CHARLES, C., BOSWELL, R.W. & FUJIWARA, T. 2011*a* Electron energy distribution of a current-free double layer: Druyvesteyn theory and experiments. *Phys. Rev. Lett*. **107**, 035002.

TAKAHASHI, K., CHARLES, C., BOSWELL, R.W., KANEKO, T. & HATAKEYAMA, R. 2007 Measurement of the energy distribution of trapped and free electrons in a current-free double layer. *Phys. Plasmas* **14** (11), 114503.

TAKAHASHI, K., CHIBA, A., KOMURO, A. & ANDO, A. 2015 Axial momentum lost to a lateral wall of a helicon plasma source. *Phys. Rev. Lett*. **114**, 195001.

TAKAHASHI, K., CHIBA, A., KOMURO, A. & ANDO, A. 2016*a* Experimental identification of an azimuthal current in a magnetic nozzle of a radiofrequency plasma thruster. *Plasma Sources Sci. Technol*. **25** (5), 055011.

TAKAHASHI, K., LAFLEUR, T., CHARLES, C., ALEXANDER, P. & BOSWELL, R.W. 2011*b* Electron diamagnetic effect on axial force in an expanding plasma: experiments and theory. *Phys. Rev. Lett*. **107**, 235001.

TAKAHASHI, K., SUGAWARA, T. & ANDO, A. 2020*b* Spatial measurement of axial and radial momentum fluxes of a plasma expanding in a magnetic nozzle. *New J. Phys*. **22** (7), 073034.

TAKAHASHI, K., TAKAO, Y. & ANDO, A. 2016*b* Neutral-depletion-induced axially asymmetric density in a helicon source and imparted thrust. *Appl. Phys. Lett*. **108** (7), 074103.

ZHANG, T., CUI, R., ZHU, W., YUAN, Q., OUYANG, J., JIANG, K., ZHANG, H., WANG, C. & CHEN, Q. 2021 Influence of neutral depletion on blue core in argon helicon plasma. *Phys. Plasmas* **28** (7), 073505.

ZHANG, Y., CHARLES, C. & BOSWELL, R. 2016 Thermodynamic study on plasma expansion along a divergent magnetic field. *Phys. Rev. Lett*. **116**, 025001.